https://doi.org/10.5194/egusphere-2023-2590
Preprint. Discussion started: 29 January 2024

Basic chemical compositions combination rules and quantitative criterion of red beds

Guangjun Cui [1,2], Jin Liao [2], Linghua Kong [2], Cuiying Zhou [2,*], Zhen Liu [2,*], Lei Yu [2], Lihai Zhang [3]

[1] Institute of Estuarine and Coastal Research/Guangdong Provincial Engineering Research Center of Coasts, Islands and Reefs, School of Ocean Engineering and Technology, Sun Yat-sen University, Guangzhou 510275, China

[2] Guangdong Engineering Research Center for Major Infrastructures Safety, Sun Yat-sen University, Guangzhou, 510275, China

[3] The University of Melbourne, Melbourne VIC 3010, Australia

*Correspondences: zhoucy@mail.sysu.edu.cn (C. Zhou), liuzh8@mail.sysu.edu.cn (Z. Liu)

Abstract

Red beds belong to slippery formations, and their rapid identification is of great significance for major scientific and engineering issues such as geological hazard risk assessment and rapid response. Existing research often identifies red beds from a qualitative or semi quantitative perspective, resulting in slow recognition speed and inaccurate recognition results, making it difficult to quickly handle landslide geological disasters. Combined with the correlation between red beds geomorphic characteristics, mineral compositions, and chemical compositions, this study established a rapid quantitative identification criterion based on the basic chemical compositions combination rules in the red beds. By collecting chemical compositions data of rocks containing red beds, a total of 241,405 groups data were collected for qualitative and quantitative comparison between multiple sets of chemical composition combinations. The results indicate that simultaneously meeting the following chemical composition combinations can serve as a quantitative criterion for distinguishing red beds from other rocks: $SiO_2+Al_2O_3 \approx 50.7\%\sim85.0\%$, $Al_2O_3/SiO_2 \approx 0.14\sim0.41$, $FeO+Fe_2O_3 \approx 0.9\%\sim7.9\%$, $Fe_2O_3/FeO \approx 1.52\sim7.70$, $K_2O+Na_2O \approx 1.6\%\sim6.8\%$, $Na_2O/K_2O \approx 0.02\sim0.43$,

https://doi.org/10.5194/egusphere-2023-2590
Preprint. Discussion started: 29 January 2024

$CaO+MgO \approx 0.8\%\sim9.2\%$. By comparing the chemical composition combinations of 15 kinds of rocks collected from China in this study, it is proven that the quantitative criterion proposed in this study are effective.

Keywords: red beds, quantitative criterion, geological disasters, rapid response, chemical compositions

1. Introduction

Red beds are widely distributed throughout the world (Chen et al. 2021; Yan et al. 2019; Zhou et al. 2023). Geological disasters occur frequently in the red beds distribution area, especially landslides, debris flows, and collapses (Chen et al. 2014). According to the characteristics of disasters such as landslides, the red beds belong to “landslide prone strata”, and the instability of slopes with weak interlayers of the red beds is particularly evident (Zhang et al. 2015). This is mainly due to the strong hydrophilicity and weak permeability of the red beds, which are prone to softening and plastic deformation under the action of water; After absorbing water, the red beds are easy to expand, and after losing water, they are easy to contract; The weathering resistance of the red beds are weak, they are easy to collapse, and their compressive and shear strength are low (Marat et al. 2022; Wang et al. 2017; Wu et al. 2018; Zhang et al. 2016). The red beds have different lithology or poor binding force with other rock strata, which can easily cause differential deformation and lead to rock mass sliding along the bedding plane (He et al. 2023; Liu et al. 2020). Therefore, the identification of rock types, especially the rapid determination of red beds, is of great significance for major scientific and engineering issues such as risk assessment and rapid response of geological disasters in red beds distribution area.

At present, the studies on red beds identification are mostly carried out from the perspectives of geomorphic characteristics, mineral compositions, and chemical compositions (Cui et al. 2022; Zhou et al. 2021). Among them, the research of geomorphic characteristics and mineral compositions mostly adopts qualitative or semi quantitative methods, and there are many such studies. For example, Rainoldi et al. (2015) identified red beds by studying the color of geomorphic characteristics and hematite in mineral compositions, and studied the mechanism of red beds bleaching. Uchida et al. (2000) distinguished red sandstone, yellowish brown sandstone, and green sandstone according to the content

https://doi.org/10.5194/egusphere-2023-2590
Preprint. Discussion started: 29 January 2024

of hematite, goethite, biotite, and muscovite in the mineral compositions, analyzed the characteristics of different rocks and pointedly protected Angkor monuments. Xue et al. (2023) distinguished red mudstone and red sandstone by quantifying the clay mineral content in the mineral compositions, in order to analyze the mechanisms and control factors of summer uplift of high-speed railway cutting. In addition, some scholars have conducted quantitative studies on the chemical compositions of red beds, and such studies are less. Hong et al. (2009) analyzed the alteration of clay minerals by studying the changes in the SiO_2/Al_2O_3 ratio in the chemical compositions of the red beds, thereby obtaining the weathering degree of the red beds. Bankole et al. (2016) studied the relationship between Fe/Mg ratio, Fe^{3+}/FeT ratio, and Cr/Fe ratio of red beds to indirectly study the oxygen content of the Paleoproterozoic. Hu et al. (2006) studied the characteristics of high Fe_2O_3 content and low FeO content in the oceanic red beds, and analyzed ancient landslides on the continental margin from the perspective of petrology. However, these studies do not distinguish between red beds and other rocks in terms of chemical compositions. The use of portable spectrometers and drone-borne multi-sensor remote sensing technique can quickly obtain the chemical compositions of rocks in geological disasters while ensuring safety (Kirsch et al. 2018; Triantafyllou et al. 2021), making it feasible to use chemical compositions as the standards to distinguish red beds from other rocks.

Therefore, the purpose of this study to develop a quantitative criterion for quickly and accurately identifying the red beds. Figure 1 shows the methodology used in this study involving the investigation of geomorphic characteristics, mineral compositions, and chemical compositions. There are few studies on identifying red beds from the perspective of chemical compositions, which is the focus of this study. Moreover, there is a close relationship between geomorphic characteristics, mineral compositions, and chemical compositions (Moonjun et al. 2017). This study first collected the data about the geomorphic characteristics, mineral content, and chemical composition of red beds and other rocks, then compared these data to obtain the basic characteristics of red beds, and finally summarized and analyzed the red beds identification criterion and verified the reliability of this criterion.

https://doi.org/10.5194/egusphere-2023-2590
Preprint. Discussion started: 29 January 2024

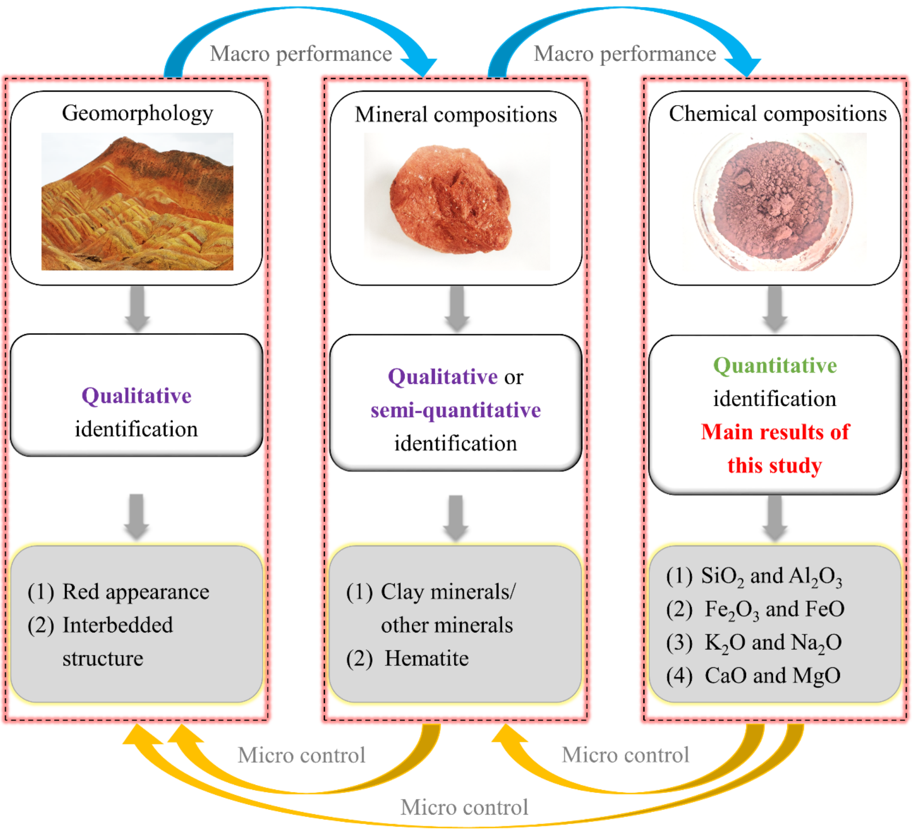

Figure 1. Methodology proposed in study for identifying red beds from geomorphic characteristics, mineral compositions, and chemical compositions.

2. Methods

2.1 Data collection

A large amount of data for red beds and other rocks was collected from previous studies and analysed from geomorphic characteristics, mineral compositions, and chemical compositions perspectives. Data were collected from the previous studies about landslides, debris flows, and collapses on the geomorphic characteristics of red beds, igneous rocks (andesite, basalt, diorite, granite), metamorphic rocks (gneiss, marble), and other sedimentary rocks (arkose, black-shale, breccia, claystone, dolomite, lignite, limestone, marl, mudstone, siliciclastic, tuff) (e.g., (Anbarasu et al. 2010; Ciftci et al. 2008; Contino et al. 2017; de Montety et al. 2007; Gokbulak and Ozcan 2008; Hale et al.

https://doi.org/10.5194/egusphere-2023-2590
Preprint. Discussion started: 29 January 2024

2021; Harp et al. 2011; He et al. 2021; Kavvadas et al. 2020; Li et al. 2016; Liu et al. 2018; Ni et al. 2015; Perez-Rey et al. 2019; San et al. 2020; Underwood et al. 2016; Wang et al. 2022; Xia et al. 2019; Zhang et al. 2015; Zhang et al. 2017)). The geomorphic characteristics of red beds investigated in this study involve the evolution process and distribution of red beds on Earth's surface, and the results were compared with that of other types of rock samples.

Previous studies have shown that there is a relationship between mineral compositions and geomorphic characteristics of red beds during the geological processes (Bankole et al. 2016). This study mainly focuses on the influence of mineral compositions on geomorphic characteristics, particularly the layered structure and color of red beds. The mineral compositions of red beds (1,536 groups data) were collected from the previous studies as shown in Supplementary Table 1 (e.g., (Bai et al. 2020; Chen et al. 2014; Jian et al. 2009; Li et al. 2023; Li et al. 2015; Li et al. 2013; Liu et al. 2020; Marat et al. 2022; Wang et al. 2018; Wang et al. 2014; Wang et al. 2017; Yao et al. 2016; Zha et al. 2022; Zhang et al. 2016; Zhang et al. 2020; Zhang et al. 2021)). These studies used semi quantitative or quantitative methods in XRD technology to statistically analyze the differences in mineral composition between different red beds (*e.g.,* quartz, feldspar, mica, hematite, clay minerals, and calcite), as detailed in the aforementioned literatures.

Moreover, previous studies have shown that the geomorphic characteristics and mineral compositions of rocks are strongly correlated to their chemical compositions (Perri et al. 2013). For example, the content of Fe_2O_3 or hematite in the red beds is higher than that in the grey beds (Hu et al. 2006). The chemical compositions of red beds (1536 groups data) with different geological ages and various lithologies such as conglomerate, sandy conglomerate, sandstone, siltstone, shale and mudstone were collected from the previous studies as shown in Supplementary Table 2 (e.g., (Gao et al. 2017; Hong et al. 2009; Jiang et al. 2022; Kong et al. 2018; Liu et al. 2007; Liu et al. 2020; Liu et al. 2006; Uchida et al. 2000; Wild et al. 2017; Xue et al. 2023; Yang et al. 2016; Zhang et al. 2008; Zhao et al. 2005; Zhu et al. 2003)). The chemical compositions of igneous rocks, including andesite (Supplementary Table 3 - 49,203 groups data. Data were downloaded from the GEOROC database (https://georoc.mpch-mainz.gwdg.de//georoc/) on 11 May 2023, using the following parameters: search = andesite.), basalt (Supplementary Table 4 - 80,365 groups data. Data were downloaded from the

https://doi.org/10.5194/egusphere-2023-2590
Preprint. Discussion started: 29 January 2024

GEOROC database on 11 May 2023, using the following parameters: search = basalt.), diorite (Supplementary Table 5 - 4,941 groups data. Data were downloaded from the GEOROC database on 11 May 2023, using the following parameters: search = diorite.), and granite (Supplementary Table 6 - 17,272 groups data. Data were downloaded from the GEOROC database on 11 May 2023, using the following parameters: search = granite.). The chemical compositions of metamorphic rocks, including gneiss (Supplementary Table 7 - 24,300 groups data. The data were downloaded from the EarthChem Portal Database (http://portal.earthchem.org/) on 20 April, 2018, using the following parameters: material = metamorphic and rock name = gneiss.) and marble (Supplementary Table 8 - 3,364 groups data. The data were downloaded from the EarthChem Portal Database on 12 May, 2023, using the following parameters: material = metamorphic and rock name = marble.). The chemical compositions of other sedimentary rocks, including arkose (Supplementary Table 9 - 682 groups data. The data were downloaded from the EarthChem Portal Database on 10 May, 2023, using the following parameters: material = sedimentary and rock name = arkose.), black-shale (Supplementary Table 10 - 305 groups data. The data were downloaded from the EarthChem Portal Database on 10 May, 2023, using the following parameters: material = sedimentary and rock name = black-shale.), breccia (Supplementary Table 11 - 1,396 groups data. The data were downloaded from the EarthChem Portal Database on 10 May, 2023, using the following parameters: material = sedimentary and rock name = breccia.), claystone (Supplementary Table 12 - 3,790 groups data. The data were downloaded from the EarthChem Portal Database on 10 May, 2023, using the following parameters: material = sedimentary and rock name = claystone.), dolomite (Supplementary Table 13 - 2,169 groups data. The data were downloaded from the EarthChem Portal Database on 6 May, 2023, using the following parameters: material = sedimentary and rock name = dolomite.), lignite (Supplementary Table 14 - 3 groups data. The data were downloaded from the EarthChem Portal Database on 24 April, 2018, using the following parameters: material = sedimentary and rock name = lignite.), limestone (Supplementary Table 15 - 9,104 groups data. The data were downloaded from the EarthChem Portal Database on 10 May, 2023, using the following parameters: material = sedimentary and rock name = limestone.), marl (Supplementary Table 16 - 142 groups data. The data were downloaded from the EarthChem Portal Database on 10 May, 2023, using the following parameters: material = sedimentary and rock name =

https://doi.org/10.5194/egusphere-2023-2590
Preprint. Discussion started: 29 January 2024

marlstone, marl.), mudstone (Supplementary Table 17 - 6,140 groups data. The data were downloaded from the EarthChem Portal Database on 10 May, 2023, using the following parameters: material = sedimentary and rock name = mudstone, mud.), siliciclastic (Supplementary Table 18 - 26,938 groups data. The data were downloaded from the EarthChem Portal Database on 10 May, 2023, using the following parameters: material = sedimentary and rock name = siliciclastic.), tuff (Supplementary Table 19 - 10,295 groups data. The data were downloaded from the EarthChem Portal Database on 6 May, 2023, using the following parameters: material = sedimentary and rock name = tuff.). Due to the high content of quartz, clay minerals, hematite, calcite, dolomite, feldspar, etc. in the red beds, the main oxide components are SiO_2, Al_2O_3, Fe_2O_3, FeO, CaO, MgO, Na_2O, and K_2O, this study mainly focuses on the differences in chemical compositions combination rules between the red beds and other rocks, such as SiO_2 and Al_2O_3, Fe_2O_3 and FeO, CaO and MgO, Na_2O and K_2O.

2.2 Criterion verification

In order to verify the proposed basic chemical compositions combination rules and quantitative criterion of red beds, 15 kinds of rocks of known rock types were selected in Guangdong, Sichuan, Hubei, Zhejiang, and Anhui provinces (Figure 2), including 12 kinds of red beds (red claystone, red mudtone, red silty mudstone, red argillaceous siltstone, red fine sandstone, red medium sandstone, red coarse sandstone, red conglomerate, etc.), limestone (1 kind), arkose (1 kind) and mudstone (1 kind).

1 red claystone

2 red mudtone 1#

3 red mudtone 2#

4 red silty mudstone

5 red argillaceous siltstone 1#

6 red argillaceous siltstone 2#

https://doi.org/10.5194/egusphere-2023-2590
Preprint. Discussion started: 29 January 2024

Figure 2. 15 kinds of rocks collected for the verification of the quantitative criterion.

These rock samples were analyzed by the MiX5 Pro handheld X-ray fluorescence element analyzer (Figure 3) of Sun Yat-sen University to check whether these elements conform to the basic chemical compositions combination rules of red beds proposed by this study. The working principle of this instrument is that a miniature X-ray source provides tube voltage and tube current, and the light tube emits continuous X-ray spectral lines. The X-rays irradiated on the sample generate X-ray fluorescence with sample characteristics, which is converted into voltage signals through detectors. On the instrument analysis interface, point the detection window towards the rock sample and press the trigger to start and stop the measurement. After amplification and data collection, the signal is processed to obtain the required test data. The instrument can detect elements with atomic number greater than or equal to 12, that is, element Na that cannot get the above attention (atomic number is 11). Therefore, the content of Na element is determined based on the median of Na_2O/K_2O of the corresponding rock in Section 3.3 and K element detected by the MiX5 Pro handheld X-ray fluorescence element analyzer. Moreover, the Fe element content obtained by this instrument is the content of Fe_2O_3+FeO. The

https://doi.org/10.5194/egusphere-2023-2590
Preprint. Discussion started: 29 January 2024

corresponding Fe_2O_3 and FeO contents are determined based on the median of Fe_2O_3/FeO of the corresponding rock in Section 3.3 and Fe_2O_3+FeO detected by the MiX5 Pro handheld X-ray fluorescence element analyzer.

Figure 3. MiX5 Pro handheld X-ray fluorescence element analyzer.

3. Results and discussions

3.1 Geomorphic characteristics of red beds

Red beds are sedimentary rocks of different geological ages (mainly Mesozoic and Cenozoic) with bedding structure typically consisting of various lithologies such as conglomerate, sandy conglomerate, sandstone, siltstone, shale and mudstone that are predominantly red in color due to the presence of ferric oxides (Yan et al. 2019). Owing to differences in depositional environments and influences of late stage geologic processes, the color of red beds can be brownish-reddish-yellow, brownish-yellow, purplish-red, brownish-red, grayish-purple and other reddish tints (Nance 2015; Yan et al. 2019), making it difficult to accurately describe using the CIELAB color space and/or Munsell color system. Bedding is a common structural feature of sedimentary rocks representing the changes in the sedimentary environment. The sandstone is one of the most common types of red beds, with a distinct reddish appearance. Compared with the red beds geomorphic characteristics, igneous rocks and metamorphic rocks do not show the two characteristics of red appearance and bedding at the same time. Basalts are reddish in appearance but does not have bedding (Cunha et al. 2005). In addition, andesites are mainly light black and have a columnar structure which is similar to that of basalts (Feizizadeh et al. 2021).

https://doi.org/10.5194/egusphere-2023-2590
Preprint. Discussion started: 29 January 2024

Most of granites are grey or light brown with a significantly different structure compared to red beds (Migon et al. 2018), while gneisses are generally characterized as a dark and light gneissic structure (Garajeh et al. 2022). Although the red color appearance and bedding structure can be used as qualitative criteria for identifying the red beds, the analysis of mineral and chemical compositions is still necessary for identifying the rocks from quantitative perspective.

3.2 Mineral compositions of red beds

Table 1 shows the statistical analysis results of mineral compositions of red beds in Supplementary Table 1. The common minerals in the red bed are quartz (median value is 40%, the same below), clay minerals (35%, including kaolinite, illite, montmorillonite, and chlorite), feldspar (10%, including K-feldspar and plagioclase), calcite (10%), mica (7%, including biotite, muscovite and sericite), and hematite (3%) according to their content. According to the average value and standard deviation, it can be seen that the content range of various minerals has significant dispersion. The ratio of the content of clay minerals to other minerals (quartz, feldspar, mica, hematite, and calcite) ranges between 0.11 to 1.50. The hematite content ranges between 1.5% and 10.0% (percentile=10%~90%), and reddish appearance of red beds is due to the abundant hematite content of the rocks. The change in mineral compositions of red beds could lead to the change in rock color which is one of the major characteristics of red beds. Furthermore, when the red beds encounter water, softening and expansion could happen because of the large amount of clay minerals in the rocks, especially the mudstone. The differences in mineral compositions of the red beds can also be quantitatively described through their chemical composition combination characteristics (Table 2).

Table 1. Mineral compositions of red beds.

Minerals	**Range (per=0%~100%)**	**Range (per=10%~90%)**	**Median value (per=50%)**	**Average value**	**Standard deviation**
Quartz (%)	2.3~94.0	21.0~69.0	40.0	42.6	18.8
Clay minerals (%)	1.0~80.0	7.8~59.0	35.0	34.1	18.6
Feldspar (%)	0.4~71.0	2.3~25.0	10.0	12.6	10.7
Mica (%)	0.1~40.8	3.0~20.0	7.0	9.2	8.2

https://doi.org/10.5194/egusphere-2023-2590
Preprint. Discussion started: 29 January 2024

Hematite (%)	0.4~25.2	1.5~10.0	3.0	5.0	4.4
Calcite (%)	0.7~97.7	3.1~23.5	10.0	12.2	10.0
Clay minerals/ Other minerals	0.01~6.00	0.11~1.50	0.61	0.76	0.66

Note: per – percentile; Other minerals – quartz, feldspar, mica, hematite, and calcite.

Table 2. Chemical composition of minerals in red beds (%).

Mineral chemical formulas	SiO_2	Al_2O_3	Fe_2O_3	FeO	CaO	MgO	Na_2O	K_2O	H_2O	CO_2
Quartz (SiO_2)	100.0									
Potassium feldspar ($KAlSi_3O_8$)	64.7	18.4						16.9		
Sodium feldspar ($NaAlSi_3O_8$)	68.8	19.4					11.8			
Calcium feldspar ($CaAl2Si_2O_8$)	43.2	36.7			20.1					
White mica ($KAl_2(AlSi_3O_{10})(OH,F)_2$)	45.2	38.4						11.8	4.1	
Biotite ($KMg_3[Si_3\ AlO_{10}](OH,F)_2$)	43.0	12.2				28.8		11.2	2.2	
Phlogopite ($K(Mg,Fe)_3AlSi_3O_{10}(F,OH)_2$)	41.6	11.8		8.3		23.2	0.5	10.9	3.6	
Hematite (Fe_2O_3)			100.0							
Calcite ($CaCO_3$)					56.0					44.0
Kaolinite ($Al_2Si_2O_5(OH)_4$)	46.6	39.5							14.0	
Illite ($K_{0.75}(Al_{1.75}R)[Si_{3.5}Al_{0.5}O_{10}](OH)_2$)	54.0	17.0		1.9		3.1		7.3	12.0	
Montmorillonite ($(Na,Ca)_{0.33}(Al,Mg)_2[Si4O_{10}](OH)_2 \cdot nH_2O$)	43.8	18.6			1.0		1.1		36.1	
Chlorite ($Y_3[Z_4O_{10}](OH)_2 \cdot Y_3(OH)_6$)	30.3	17.1		15.1		25.4			12.1	

Note: Data collected from http://webmineral.com/ and https://www.mindat.org/.

3.3 Chemical composition characteristics of red beds

Figures 4~5 are mainly used to qualitatively analyze the differences in chemical compositions between the red beds and other rocks through scatter plots. The area surrounded by black dashed lines is the area where the red beds data points are located. To better distinguish various rock data points, the distribution areas of various rock data are shown on the right side of the figure, and the corresponding colored dashed ellipses are used to indicate the distribution areas in the dataset. Figure 4 shows the comparison of SiO_2 and Al_2O_3, FeO and Fe_2O_3, K_2O and Na_2O, CaO and MgO contents in red beds, igneous rocks, and metamorphic rocks, respectively. Figure 5 shows the comparison of SiO_2 and Al_2O_3, FeO and Fe_2O_3, K_2O and Na_2O, CaO and MgO contents in red beds and other sedimentary rocks respectively.

The content of SiO_2 in the red beds is about 30%~80%, Al_2O_3 is about 8%~30%, Fe_2O_3 is about

0%~10%, FeO is about 0%~3%, K_2O is about 0%~10%, Na_2O is about 0%~2.5%, CaO is about 0%~10%, and MgO is about 0%~5%. Compared with igneous rocks, metamorphic rocks, and other sedimentary rocks, the content of each chemical composition of the red beds has three relationships with the content of corresponding chemical composition of other rocks: inclusion relationship (the data distribution range of one rock completely covers and is larger than the data range of the other rock), intersection relationship (the data distribution range of one rock intersects with the data distribution range of another rock), and mutual difference relationship (the data distribution range of one rock does not intersect at all with the data distribution range of another rock). The distribution range of SiO_2 and Al_2O_3 content in the red beds includes the distribution range of SiO_2 and Al_2O_3 content in 9 types of rocks, namely andesite, basalt, diorite, granite, black shale, claystone, mudstone, siliciclastic, and tuff. The distribution range of SiO_2 and Al_2O_3 content in the red beds intersects with that in breccia, lignite, and marl. The distribution range of SiO_2 and Al_2O_3 content in gneiss, marble, arkose, dolomite, and limestone is different from that in the red beds. The distribution range of Fe_2O_3 and FeO content in the red beds includes the distribution range of Fe_2O_3 and FeO content in granite, marble, and lignite. The distribution range of Fe_2O_3 and FeO content in the red beds intersects with that in 8 kinds of rocks, namely, andesite, basalt, diorite, breccia, claystone, dolomite, limestone, and mudstone. The distribution range of Fe_2O_3 and FeO content in gneiss, arkose, black shale, siliciclastic, and tuff is different from that in the red beds. The distribution range of K_2O and Na_2O content in the red beds includes the distribution range of K_2O and Na_2O content in lignite. The distribution range of K_2O and Na_2O content in the red beds intersects with that in 15 kinds of rocks, including andesite, basalt, diorite, granite, marble, arkose, black shale, breccia, claystone, dolomite, limestone, marl, mudstone, siliciclastic, and tuff. The distribution range of K_2O and Na_2O content in gneiss is different from that in the red beds. The distribution range of CaO and MgO content in the red beds includes the distribution range of CaO and MgO content in granite, black shale, and lignite. The distribution range of CaO and MgO content in the red beds intersects with that in 13 types of rocks, including andesite, basalt, diorite, gneiss, arkose, breccia, claystone, dolomite, limestone, marl, mudstone, siliciclastic, and tuff. The distribution range of CaO and MgO content in marble is different from that in the red beds. Therefore, from a qualitative perspective, it can be seen that the red beds differ in chemical composition from 8

https://doi.org/10.5194/egusphere-2023-2590
Preprint. Discussion started: 29 January 2024

kinds of rocks, including gneiss, marble, arkose, dolomite, limestone, black-shale, siliciclastic, and tuff, and also intersects with other rocks to varying degrees. But this is not enough as a criterion to determine the difference between red beds and other rocks.

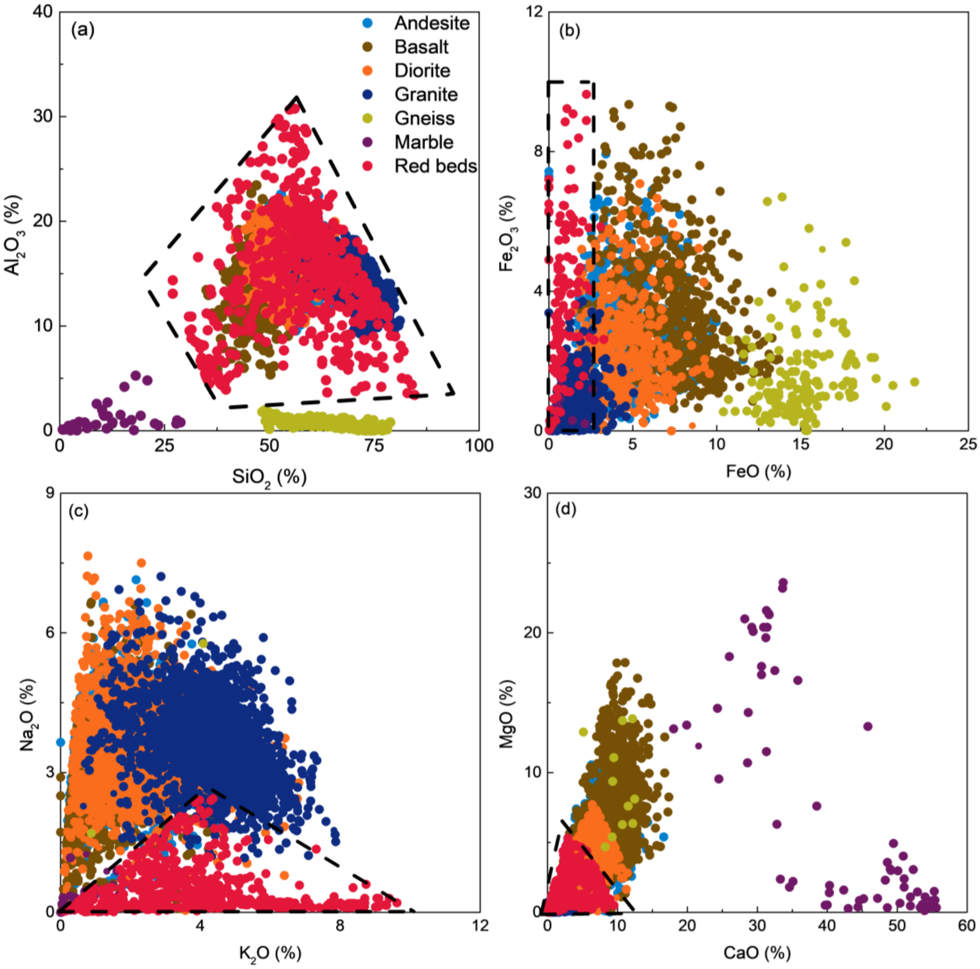

Figure 4. Comparison of (a) SiO_2 and Al_2O_3, (b) FeO and Fe_2O_3, (c) K_2O and Na_2O, (d) CaO and MgO contents in red beds, igneous rock, and metamorphic rocks, respectively.

https://doi.org/10.5194/egusphere-2023-2590
Preprint. Discussion started: 29 January 2024

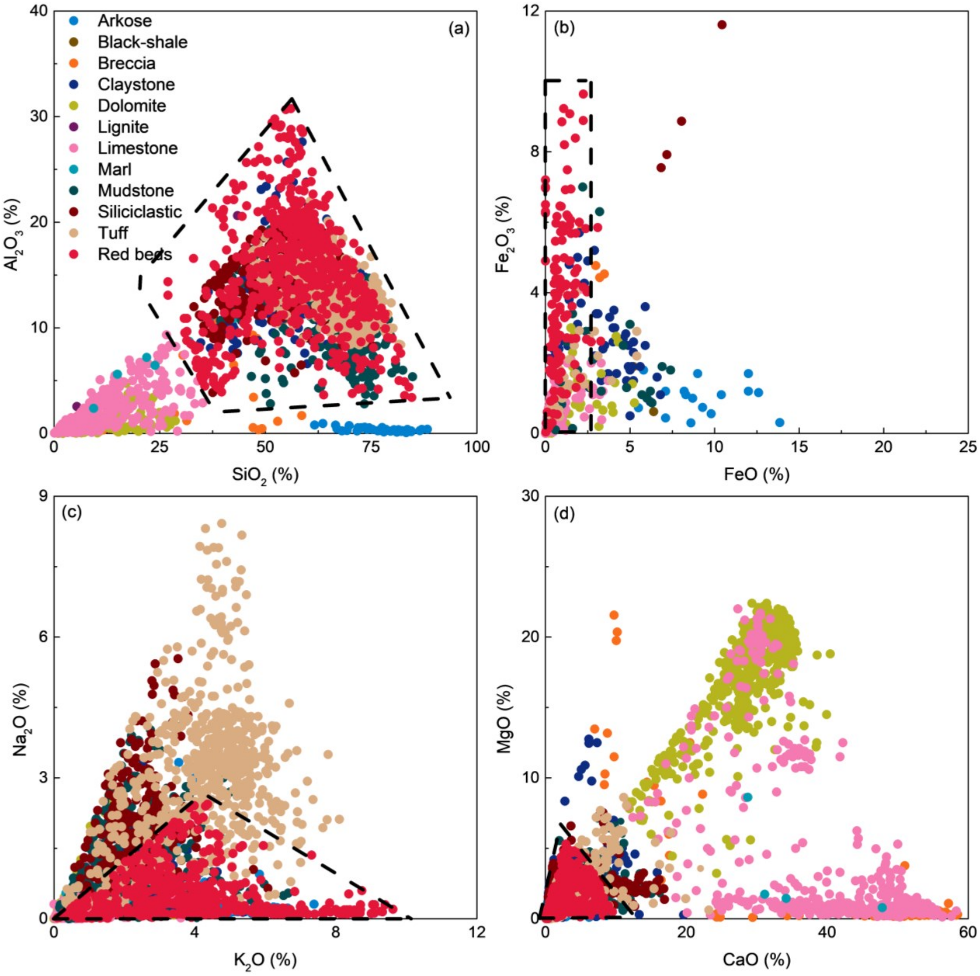

Figure 5. Comparison of (a) SiO_2 and Al_2O_3, (b) FeO and Fe_2O_3, (c) K_2O and Na_2O, (d) CaO and MgO contents in red beds and other sedimentary rocks respectively.

Figures 6~7 mainly analyze the differences in chemical compositions between red beds and other rocks through further data statistics and box plots of the scatter plots mentioned above, and propose quantitative identification criterion for the red beds chemical compositions combination. The red dashed box in the figure represents rocks that differ from the red beds data, while the black dashed box represents rocks that intersect less than 25% with the red beds data. The data collected in section 2.1 comes from published papers or databases, and its accuracy and robustness have been explained in

https://doi.org/10.5194/egusphere-2023-2590
Preprint. Discussion started: 29 January 2024

relevant literature. In order to ensure the exclusion of outliers in the box plots mentioned above during the analysis of this study. The horizontal gray dashes corresponding to the red beds box chart represent 10% percentile (the same below), lower quartile (25% percentile), median (50% percentile), upper quartile (75% percentile), and 90% percentile in the red beds data from bottom to top. Figure 6 shows the chemical compositions combination comparison of SiO_2+Al_2O_3 (total content, the same below) and Al_2O_3/SiO_2 (content ratio, the same below), FeO+Fe_2O_3 and Fe_2O_3/FeO, K_2O+Na_2O and Na_2O/K_2O, CaO+MgO and MgO/CaO in red beds, igneous rock, and metamorphic rocks, respectively. Figure 7 respectively shows the chemical compositions combination comparison of SiO_2+Al_2O_3 and Al_2O_3/SiO_2, FeO+Fe_2O_3 and Fe_2O_3/FeO, K_2O+Na_2O and Na_2O/K_2O, CaO+MgO and MgO/CaO in red beds and other sedimentary rocks.

The SiO_2+Al_2O_3 content in the red beds is 54.7%~85.0% (10%~90% percentile, the same below), the Al_2O_3/SiO_2 ratio is 0.14~0.41, the FeO+Fe_2O_3 content is 0.9%~7.9%, the Fe_2O_3/FeO ratio is 1.52~7.70, the K_2O+Na_2O content is 1.6%~6.8%, the Na_2O/K_2O ratio is 0.02~0.43, the CaO+MgO content is 0.8%~9.2%, and the MgO/CaO ratio is 0.16~1.57. By comparing the content of SiO_2+Al_2O_3, the red beds are distinct or have small intersections (less than 25%, the same below) with granite, marble, dolomite, lignite, limestone, and marl. By comparing the Al_2O_3/SiO_2 ratio, it is found that the red beds are distinct or have small intersections with gneiss, marble, arkose, and lignite. By comparing the content of FeO+Fe_2O_3, it is found that the red beds are distinct or have small intersections with basalt, gneiss, arkose, and siliciclastic. By comparing the Fe_2O_3/FeO ratio, it is found that the red beds are distinct or have small intersections with andesite, basalt, diorite, granite, gneiss, marble, arkose, black shale, dolomite, mudstone, siliclastic, and tuff. Through the comparison of K_2O+Na_2O content, the red beds are distinct or have small intersections with granite, marble, breccia, dolomite, and limestone. By comparing the Na_2O/K_2O ratio, the red beds are distinct or have small intersections with andesite, basalt, diorite, gneiss, lignite, siliciclastic, and tuff. Through the comparison of CaO+MgO content, the red beds are distinct or have small intersections with andesite, basalt, gneiss, marble, breccia, dolomite, limestone, and marl. By comparing the MgO/CaO ratio, it is difficult to distinguish the red beds from other rocks.

https://doi.org/10.5194/egusphere-2023-2590
Preprint. Discussion started: 29 January 2024

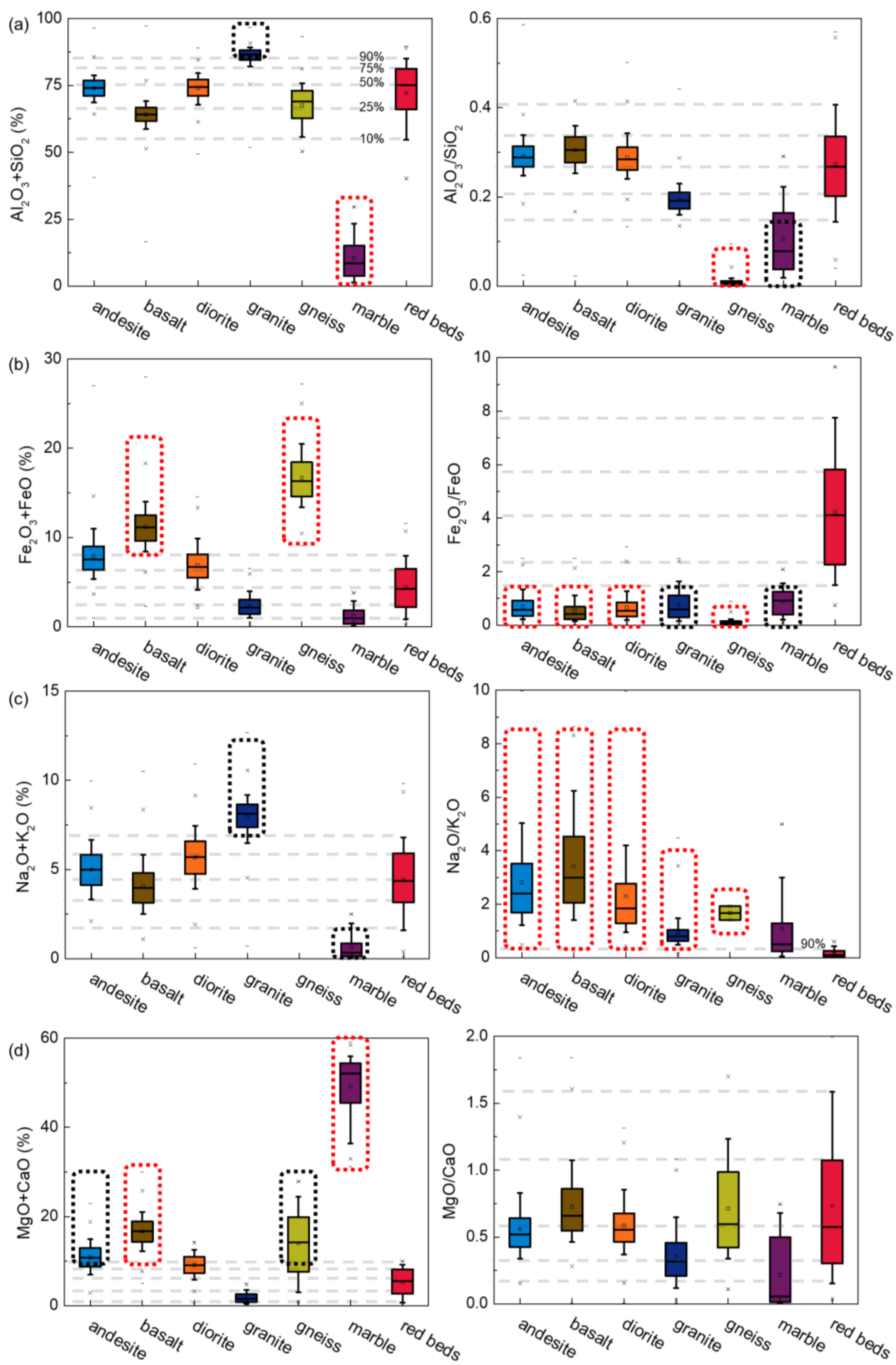

Figure 6. Chemical compositions comparison of (a) SiO_2+Al_2O_3, Al_2O_3/SiO_2, (b) FeO+Fe_2O_3, Fe_2O_3/FeO, (c) K_2O+Na_2O, Na_2O/K_2O, (d) CaO+MgO, MgO/CaO in red beds, igneous rock, and metamorphic rocks.

https://doi.org/10.5194/egusphere-2023-2590
Preprint. Discussion started: 29 January 2024

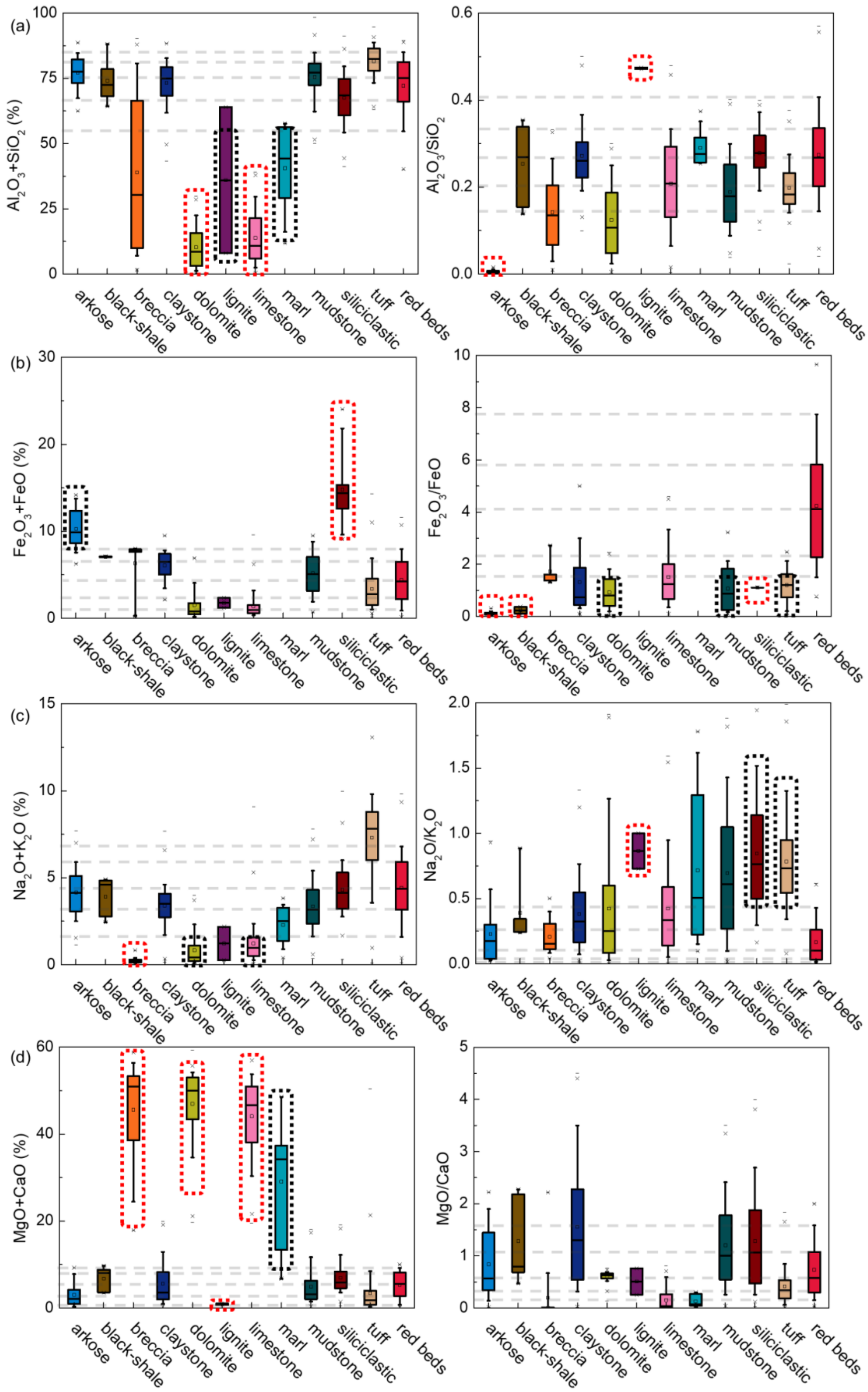

Figure 7. Chemical compositions comparison of (a) $SiO_2+Al_2O_3$, Al_2O_3/SiO_2, (b) $FeO+Fe_2O_3$, Fe_2O_3/FeO, (c) K_2O+Na_2O, Na_2O/K_2O, (d) $CaO+MgO$, MgO/CaO in red beds and other sedimentary rocks.

https://doi.org/10.5194/egusphere-2023-2590
Preprint. Discussion started: 29 January 2024

In summary, there are differences in chemical compositions between red beds and other rocks, and the use of chemical compositions combination rules can serve as a quantitative criterion for identifying red beds. Simultaneously meeting the following chemical compositions combinations as a quantitative criterion to distinguish red beds with different geological ages and various lithologies from other rocks: $SiO_2+Al_2O_3 \approx 50.7\%\sim85.0\%$, $Al_2O_3/SiO_2 \approx 0.14\sim0.41$, $FeO+Fe_2O_3 \approx 0.9\%\sim7.9\%$, $Fe_2O_3/FeO \approx 1.52\sim7.70$, $K_2O+Na_2O \approx 1.6\%\sim6.8\%$, $Na_2O/K_2O \approx 0.02\sim0.43$, $CaO+MgO \approx 0.8\%\sim9.2\%$.

3.4 Red beds identification quantization criterion verification

The chemical composition combinations of the 15 selected rocks in this study are shown in Table 3. The chemical composition combinations of 12 kinds of red beds are all within the scope of the quantitative criterion. There are some chemical composition combinations of the 3 non-red beds sedimentary rocks that are outside the scope of the red beds quantitative criterion (the numbers in bold and underlined in the table). For example, the content of $SiO_2+Al_2O_3$, $FeO+Fe_2O_3$, K_2O+Na_2O in limestone is lower than the range of quantification criterion, while the content of CaO+MgO in limestone is higher than the range of quantification criterion; Fe_2O_3/FeO and K_2O+Na_2O in arkose are below the quantification criterion; $SiO_2+Al_2O_3$ and Na_2O/K_2O in mudstone are higher than the quantification criterion, while Fe_2O_3/FeO and K_2O+Na_2O are lower than the quantification criterion. This is consistent with the research results in Figure 7, once again proving the reliability of the quantification criterion proposed in this study.

Table 3. Chemical composition combinations of 15 kinds of rocks.

No.	SiO_2 (%)	Al_2O_3 (%)	Fe_2O_3 (%)	FeO (%)	Na_2O (%)	K_2O (%)	MgO (%)	CaO (%)	$SiO_2+Al_2O_3$ (%)	Al_2O_3/SiO_2	$FeO+Fe_2O_3$ (%)	Fe_2O_3/FeO	K_2O+Na_2O (%)	Na_2O/K_2O	CaO+MgO (%)
1	43.3	15.0	2.9	0.7	0.2	1.9	3.3	1.1	58.3	0.35	3.6	4.12	2.1	0.10	4.4
2	45.8	18.3	4.1	1.0	0.3	2.6	2.3	0.0	64.1	0.40	5.1	4.12	2.9	0.10	2.3
3	40.1	15.5	3.7	0.9	0.2	2.1	3.6	0.0	55.6	0.39	4.6	4.12	2.3	0.10	3.6
4	48.8	14.3	3.1	0.7	0.3	2.9	2.9	6.1	63.1	0.29	3.8	4.12	3.2	0.10	9.0

https://doi.org/10.5194/egusphere-2023-2590
Preprint. Discussion started: 29 January 2024

5	62.0	15.8	2.7	0.6	0.3	3.2	3.1	0.0	77.8	0.26	3.3	4.12	3.5	0.10	3.1
6	42.8	9.4	1.6	0.4	0.2	1.5	0.4	4.1	52.2	0.22	2.0	4.12	1.7	0.10	4.5
7	52.2	17.1	1.5	0.4	0.2	2.3	2.5	0.0	69.3	0.33	1.9	4.12	2.5	0.10	2.5
8	58.3	18.6	1.6	0.4	0.2	1.9	4.0	0.8	76.9	0.32	2.0	4.12	2.1	0.10	4.8
9	39.9	11.2	1.3	0.3	0.2	1.5	3.9	0.0	51.1	0.28	1.4	4.12	1.7	0.10	3.9
10	48.2	9.6	1.0	0.2	0.2	2.4	3.5	1.9	57.8	0.20	1.2	4.12	2.6	0.10	5.4
11	50.5	14.2	2.1	0.5	0.2	2.3	0.8	5.1	64.7	0.28	2.6	4.12	2.5	0.10	5.9
12	45.1	8.4	3.5	0.8	0.2	2.0	2.3	1.6	53.5	0.19	4.3	4.12	2.2	0.10	3.9
13	13.6	2.3	0.1	0.1	0.2	0.5	3.2	39.6	***15.9***	0.17	***0.2***	1.23	***0.7***	0.33	***42.8***
14	56.9	14.9	0.3	2.3	0.2	1.3	3.3	1.1	71.8	0.26	2.6	0.11	***1.5***	0.18	4.4
15	69.7	21.2	0.6	0.7	0.3	0.5	0.9	0.0	***90.9***	0.30	1.3	0.87	***0.8***	0.61	0.9

3.5 Research results application methods

Figure 8 shows the application methods of the research results. According to the methods for emergency management of landslide geological disasters (Fu et al. 2021), landslide risk assessment (including risk identification, risk analysis, and risk assessment) and risk management (developing and selecting treatment plans, as well as planning, implementing, and evaluating treatment methods) need to be carried out before the landslide occurs. In the field of engineering geology, risk identification is the most important prerequisite for landslide emergency response. Red beds is the slippery layer that needs to be identified in risk identification.

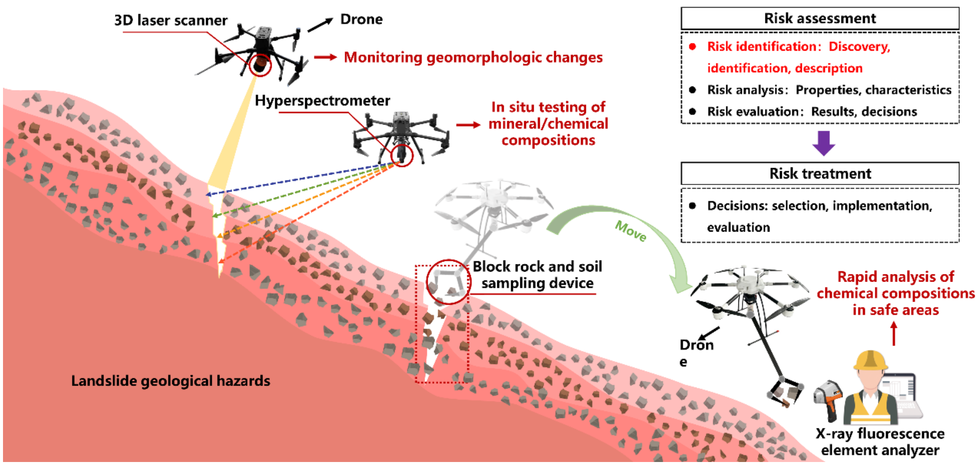

Figure 8. Research results used for risk identification.

https://doi.org/10.5194/egusphere-2023-2590
Preprint. Discussion started: 29 January 2024

At present, the commonly used risk identification method is to use drones to carry image capture devices for three-dimensional reconstruction of slope images, determine the volume of landslide accumulation, and determine the shape changes of the slope (Chen et al. 2020; Fu et al. 2021), which can be also used for mountain rescue (Wankmuller et al. 2021). Based on the drone technology, combined with the Optech Polaris LR 3D laser scanner and the HY-9070 hyperspectral analyzer of Sun Yat-sen University, the landslide shape change and remote monitoring of mineral and chemical compositions can be realized to identify whether it is a red beds landslide. It can also use a drone equipped with a block rock and soil sampling device to collect representative blocks of rock and soil within cracks to a safe area, and then use the MiX5 Pro handheld X-ray fluorescence element analyzer for rapid analysis. Therefore, the research results can be used for rapid identification of red beds, achieving risk assessment and rapid response of geological disasters such as landslides.

4. Conclusions

(1) In response to the rapid identification of red beds in geological disaster emergency response, a rapid quantitative identification criterion based on the basic chemical compositions combination rules of red beds has been established, taking into account the correlation between red beds geomorphic characteristics, mineral compositions, and chemical compositions.

(2) The results indicate that the red beds in the geomorphic characteristics has obvious interlayer characteristics and its appearance is red. In mineral composition, the ratio of clay minerals to other minerals of red beds ranges from 0.11 to 1.50, and the content of hematite of red beds ranges from 1.5% to 10.0%. The following chemical composition combinations can be used as red beds quantification criterion: $SiO_2+Al_2O_3 \approx 50.7\%{\sim}85.0\%$, $Al_2O_3/SiO_2 \approx 0.14{\sim}0.41$, $FeO+Fe_2O_3 \approx 0.9\%{\sim}7.9\%$, $Fe_2O_3/FeO \approx 1.52{\sim}7.70$, $K_2O+Na_2O \approx 1.6\%{\sim}6.8\%$, $Na_2O/K_2O \approx 0.02{\sim}0.43$, $CaO+MgO \approx 0.8\%{\sim}9.2\%$. The reliability of the quantitative criterion proposed by this study was verified by collecting 15 kinds of rocks and analyzing their chemical composition combinations.

(3) The combination of research results with existing landslide geological hazard risk identification techniques can effectively carry out rapid response to geological disasters, which is very important for

https://doi.org/10.5194/egusphere-2023-2590
Preprint. Discussion started: 29 January 2024

emergency response to geological disasters. Moreover, the research results can also be applied to the quantitative identification of red beds in other fields such as resources, ecology, environment, energy, materials, etc.

Declarations

Availability of data and materials

The data that support the findings of this study are available in supplementary materials.

Competing interests

The authors declare no conflict of interest. The funders had no role in the design of the study; in the collection, analyses, or interpretation of data; in the writing of the manuscript, or in the decision to publish the results.

Funding

The research is supported by the National Natural Science Foundation of China (NSFC) (Grant Numbers: 42293354, 42293351, 42293355, 42277131, 41977230).

Authors' contributions

Conceptualization, C.Z. and Z.L.; methodology, G.C. and Z.L.; software, G.C. and L.K.; validation, G.C., L.K., and Z.L.; formal analysis, C.Z. and Z.L.; investigation, G.C., J.L., and L.Y.; resources, G.C. and L.K.; data curation, G.C., J.L., L.Y. and L.K.; writing—original draft preparation, G.C. and L.K.; writing—review and editing, G.C., Z.L., and L.Z.; visualization, L.Y.; supervision, Z.L. and L.Z.; project administration, C.Z.; funding acquisition, C.Z. All authors have read and agreed to the published version of the manuscript.

Acknowledgments

The authors would like to thank the anonymous reviewers for their very constructive and helpful comments.

Supplementary Materials

Supplementary Table 1: Mineral compositions of the red beds.

Supplementary Table 2: Chemical compositions of the red beds.

Supplementary Table 3: Chemical compositions of the andesite.

https://doi.org/10.5194/egusphere-2023-2590
Preprint. Discussion started: 29 January 2024

Supplementary Table 4: Chemical compositions of the basalt.

Supplementary Table 5: Chemical compositions of the diorite.

Supplementary Table 6: Chemical compositions of the granite.

Supplementary Table 7: Chemical compositions of the gneiss.

Supplementary Table 8: Chemical compositions of the marble.

Supplementary Table 9: Chemical compositions of the arkose.

Supplementary Table 10: Chemical compositions of the black-shale.

Supplementary Table 11: Chemical compositions of the breccia.

Supplementary Table 12: Chemical compositions of the claystone.

Supplementary Table 13: Chemical compositions of the dolomite.

Supplementary Table 14: Chemical compositions of the lignite.

Supplementary Table 15: Chemical compositions of the limestone.

Supplementary Table 16: Chemical compositions of the marl.

Supplementary Table 17: Chemical compositions of the mudstone.

Supplementary Table 18: Chemical compositions of the siliciclastic.

Supplementary Table 19: Chemical compositions of the tuff.

References

Anbarasu, K., Sengupta, A., Gupta, S. & Sharma, S.P. 2010. Mechanism of activation of the Lanta Khola landslide in Sikkim Himalayas. Landslides, **7**, 135-147, doi: 10.1007/s10346-009-0193-0.

Bai, Y., Shan, R., Ju, Y., Wu, Y., Tong, X., Han, T. & Dou, H. 2020. Experimental study on the strength, deformation and crack evolution behaviour of red sandstone samples containing two ice-filled fissures under triaxial compression. Cold Regions Science and Technology, **174**, doi: 10.1016/j.coldregions.2020.103061.

Bankole, O.M., Albani, A.E., Meunier, A., Rouxel, O.J., Oisgauthier-Lafaye, F. & Bekker, A. 2016. Origin of Red Beds in the Paleoproterozoic Franceville Basin, Gabon, and Implications for Sandstone-Hosted Uranium Mineralization. American Journal of Science, **316**, 839-872, doi: 10.2475/09.2016.02.

Chen, J., Dai, F., Xu, L., Chen, S., Wang, P., Long, W. & Shen, N. 2014. Properties and microstructure of a natural slip zone in loose deposits of red beds, southwestern China. Engineering Geology, **183**, 53-64, doi: 10.1016/j.enggeo.2014.10.004.

Chen, S.J., Xiang, C.C., Kang, Q., Zhong, W., Zhou, Y.L. & Liu, K. 2020. Accurate landslide detection leveraging UAV-based aerial remote sensing. Iet Communications, **14**, 2434-2441, doi: 10.1049/iet-com.2019.1115.

Chen, Z.Y., Männik, P., Fan, J.X., Wang, C.Y., Chen, Q., Sun, Z.Y., Chen, D.Y. & Li, C. 2021. Age of the Silurian Lower Red Beds in South China: Stratigraphical Evidence from the Sanbaiti Section. Journal of Earth Science, **32**, 524-533, doi: 10.1007/s12583-020-1350-6.

Ciftci, E., Hogan, J.P., Kolayli, H. & Cadirli, E. 2008. Natrolitite, an unusual rock - Occurrence and petrographic and geochemical characteristics (eastern Turkey). Clays and Clay Minerals, **56**, 207-221, doi: 10.1346/Ccmn.2008.0560206.

Contino, A., Bova, P., Esposito, G., Giuffre, I. & Monteleone, S. 2017. Historical analysis of rainfall-triggered rockfalls: the case study of the disaster of the ancient hydrothermal Sclafani Spa (Madonie Mts, northern-central Sicily, Italy) in 1851. Natural Hazards and Earth System Sciences, **17**, 2229-2243, doi: 10.5194/nhess-17-2229-2017.

Cui, G., Zhou, C., Liu, Z., Xia, C. & Zhang, L. 2022. The synthesis of soft rocks based on physical and mechanical properties of red mudstone. International Journal of Rock Mechanics and Mining Sciences, **151**, 105037, doi: https://doi.org/10.1016/j.ijrmms.2022.105037.

Cunha, P., Marques, J., Curi, N., Pereira, G.T. & Lepsch, I.F. 2005. Geomorphic surfaces and latosol (oxisol) characteristics on a sandstone/basalt sequence from the Jaboticabal region, Sao Paulo State, Brazil. Revista Brasileira De Ciencia Do Solo, **29**, 81-90, doi: Doi 10.1590/S0100-06832005000100009.

de Montety, V., Marc, V., Emblanch, C., Malet, J.P., Bertrand, C., Maquaire, O. & Bogaard, T.A. 2007. Identifying the origin of groundwater and flow processes in complex landslides affecting black marls: insights from a hydrochemical survey. Earth Surface Processes and Landforms, **32**, 32-48, doi: 10.1002/esp.1370.

Feizizadeh, B., Garajeh, M.K., Blaschke, T. & Lakes, T. 2021. An object based image analysis applied for volcanic and glacial landforms mapping in Sahand Mountain, Iran. Catena, **198**, doi: 10.1016/j.catena.2020.105073.

Fu, L., Zhu, J., Li, W.-l., You, J.-g. & Hua, Z.-y. 2021. Fast estimation method of volumes of landslide deposit by the 3D reconstruction of smartphone images. Landslides, **18**, 3269-3278, doi: 10.1007/s10346-021-01702-9.

Gao, F., Wu, X. & Deng, R. 2017. The distribution of red beds and analysis on engineering characteristics of mudstone in Guangxi. Journal of Geological Hazards and Environment Preservation, **28**, 48-52.

Garajeh, M.K., Feizizadeh, B., Blaschke, T. & Lakes, T. 2022. Detecting and mapping karst landforms using object-based image analysis: Case study: Takht-Soleiman and Parava Mountains, Iran. The Egyptian Journal of Remote Sensing and Space Science, **25**, 473-489, doi: https://doi.org/10.1016/j.ejrs.2022.03.009.

Gokbulak, F. & Ozcan, M. 2008. Hydro-physical properties of soils developed from different parent materials. Geoderma, **145**, 376-380, doi: 10.1016/j.geoderma.2008.04.006.

Hale, S., Ries, X., Jaeggi, D. & Blum, P. 2021. Mechanical and hydraulic properties of the excavation damaged zone (EDZ) in the Opalinus Clay of the Mont Terri rock laboratory, Switzerland. Solid Earth, **12**, 1581-1600, doi: 10.5194/se-12-1581-2021.

Harp, E.L., Dart, R.L. & Reichenbach, P. 2011. Rock fall simulation at Timpanogos Cave National Monument, American Fork Canyon, Utah, USA. Landslides, **8**, 373-379, doi: 10.1007/s10346-010-0251-7.

He, J., Niu, F., Luo, F., Jiang, H., He, P. & Ju, X. 2023. Mechanical properties and modified binary-medium constitutive model for red-bed soft rock subjected to freeze-thaw cycles. Cold Regions Science and Technology, **209**, doi: 10.1016/j.coldregions.2023.103803.

He, K., Ma, G.T. & Hu, X.W. 2021. Formation mechanisms and evolution model of the tectonic-related ancient giant basalt landslide in Yanyuan County, China. Natural Hazards, **106**, 2575-2597, doi: 10.1007/s11069-021-04555-6.

Hong, H., Li, Z. & Xiao, P. 2009. Clay Mineralogy Along the Laterite Profile in Hubei, South China: Mineral Evolution and Evidence for Eolian Origin. Clays and Clay Minerals, **57**, 602-615, doi: 10.1346/Ccmn.2009.0570508.

Hu, X., Wang, C., Li, X. & Luba, J. 2006. Upper Cretaceous oceanic red beds in southern Tibet: Lithofacies, environments and colour origin. Science in China Series D-Earth Sciences, **49**, 785-795, doi: 10.1007/s11430-006-0785-7.

Jian, W.X., Wang, Z.J. & Yin, K.L. 2009. Mechanism of the Anlesi landslide in the Three Gorges Reservoir, China. Engineering Geology, **108**, 86-95, doi: 10.1016/j.enggeo.2009.06.017.

Jiang, H., Xia, Y., Li, J., Liu, S., Zhang, M. & Wang, Y. 2022. Controlling the Iron Migration Mechanism for the Cretaceous Sediment Color Variations in Sichuan Basin, China. Acs Omega, **7**, 480-495, doi: 10.1021/acsomega.1c04893.

Kavvadas, M., Roumpos, C. & Schilizzi, P. 2020. Stability of Deep Excavation Slopes in Continuous Surface Lignite Mining Systems. Geotechnical and Geological Engineering, **38**, 791-812, doi: 10.1007/s10706-019-01066-x.

Kirsch, M., Lorenz, S., Zimmermann, R., Tusa, L., Mockel, R., Hodl, P., Booysen, R., Khodadadzadeh, M. & Gloaguen, R. 2018. Integration of Terrestrial and Drone-Borne Hyperspectral and Photogrammetric Sensing Methods for Exploration Mapping and Mining Monitoring. Remote Sensing, **10**, doi: 10.3390/rs10091366.

Kong, L.W., Zeng, Z.X., Bai, W. & Wang, M. 2018. Engineering geological properties of weathered swelling mudstones and their effects on the landslides occurrence in the Yanji section of the Jilin-Hunchun high-speed railway. Bulletin of Engineering Geology and the Environment, **77**, 1491-1503, doi: 10.1007/s10064-017-1096-2.

Li, A., Deng, H., Zhang, H., Liu, H. & Jiang, M. 2023. The shear-creep behavior of the weak interlayer mudstone in a red-bed soft rock in acidic environments and its modeling with an improved Burgers model. Mechanics of Time-Dependent Materials, **27**, 1-18, doi: 10.1007/s11043-021-09523-y.

Li, J., Xu, Q., Hu, Z., Liu, H., Zhang, Q., Lu, Y. & Wang, S. 2015. Experimental research on softening of undisturbed saturated slip soil in eastern of Sichuan province red bed. Chinese Journal of Rock Mechanics and Engineering, **34**, 4333-4342.

Li, S., Chen, J. & Yi, G. 2013. Experimental study on the relationship between micro-characteristics and compressive strength of the red bed rock. Geotechnical Investigation and Surveying, **41**, 1-5.

Li, X.N., Zhu, B.L. & Wu, X.Y. 2016. Swelling characteristics of soils derived from black shales heightened by cations in Northern Chongqing, China. Journal of Mountain Science, **13**, 1107-1119, doi: 10.1007/s11629-015-3576-9.

Liu, C., He, C. & He, M. 2007. Engineering geology study on failure of red beds slopes along railway in the west of Hunan Province. The Chinese Journal of Geological Hazard and Control, **18**, 58-62.

Liu, J., Wei, J.H., Hu, H., Wu, J.M., Sun, S.R. & Kanungo, D.P. 2018. Research on the engineering geological conditions and stability evaluation of the B2 talus slide at the Jin'an Bridge hydropower station, China. Bulletin of Engineering Geology and the Environment, **77**, 105-125, doi: 10.1007/s10064-017-1005-8.

Liu, J., Xu, Q., Wang, S., Siva Subramanian, S., Wang, L. & Qi, X. 2020. Formation and chemo-mechanical characteristics of weak clay interlayers between alternative mudstone and sandstone sequence of gently inclined landslides in Nanjiang, SW China. Bulletin of Engineering Geology and the Environment, **79**, 4701-4715, doi: 10.1007/s10064-020-01859-y.

Liu, X., Zhao, M., Su, Y. & Long, Y. 2006. Grey Correlation Analysis of Slake Durability of Red Bed Weak Rock. Journal of Hunan University (Natural Sciences), **33**, 16-20.

Marat, A.R., Tamas, T., Samsudean, C. & Gheorghiu, R. 2022. Physico-mechanical and mineralogical investigations of red bed slopes (Cluj-Napoca, Romania). Bulletin of Engineering Geology and the Environment, **81**, doi: ARTN 78
10.1007/s10064-021-02542-6.

Migon, P., Woo, K.S. & Kasprzak, M. 2018. Landform Recognition in Granite Mountains in East Asia (Seoraksan, Republic of Korea, and Huangshan and Sanqingshan, China) - a Contribution of Geomorphology to the Unesco World Heritage. Quaestiones Geographicae, **37**, 103-114, doi: 10.2478/quageo-2018-0008.

Moonjun, R., Shrestha, D.P., Jetten, V.G. & van Ruitenbeek, F.J.A. 2017. Application of airborne gamma-ray imagery to assist soil survey: A case study from Thailand. Geoderma, **289**, 196-212, doi: 10.1016/j.geoderma.2016.10.035.

Nance, H.S. 2015. Interfingering of evaporites and red beds: an example from the queen/grayburg formation, Texas. Sedimentary Geology, **56**, 357-381.

Ni, L.T., Zhong, J.H., Shao, Z.F., Li, Y., Mao, C. & Liu, S.X. 2015. Characteristics, Genesis, and Sedimentary Environment of Duplex-Like Structures in the Jurassic Sediments of Western Qaidam Basin, China. Journal of Earth Science, **26**, 677-689, doi: 10.1007/s12583-015-0578-2.

Perez-Rey, I., Riquelme, A., Gonzalez-deSantos, L.M., Estevez-Ventosa, X., Tomas, R. & Alejano, L.R. 2019. A multi-approach rockfall hazard assessment on a weathered granite natural rock slope. Landslides, **16**, 2005-2015, doi: 10.1007/s10346-019-01208-5.

Perri, F., Critelli, S., Martín-Algarra, A., Martín-Martín, M., Perrone, V., Mongelli, G. & Zattin, M. 2013. Triassic redbeds in the Malaguide Complex (Betic Cordillera - Spain): Petrography, geochemistry and geodynamic implications. Earth-Science Reviews, **117**, 1-28, doi: 10.1016/j.earscirev.2012.11.002.

Rainoldi, A.L., Franchini, M., Beaufort, D., Mozley, P., Giusiano, A., Nora, C., Patrier, P., Impiccini, A. & Pons, J. 2015. Mineral reactions associated with hydrocarbon paleomigration in the Huincul High, Neuquen Basin, Argentina. Geological Society of America Bulletin, **127**, 1711-1729, doi: 10.1130/B31201.1.

San, N.E., Topal, T. & Akin, M.K. 2020. Rockfall Hazard Assessment Around Ankara Citadel (Turkey) Using Rockfall Analyses and Hazard Rating System. Geotechnical and Geological Engineering, **38**, 3831-3851, doi: 10.1007/s10706-020-01261-1.

Triantafyllou, A., Mattielli, N., Clerbois, S., Da Silva, A.C., Kaskes, P., Claeys, P., Devleeschouwer, X. & Brkojewitsch, G. 2021. Optimizing multiple non-invasive techniques (PXRF, pMS, IA) to characterize

https://doi.org/10.5194/egusphere-2023-2590
Preprint. Discussion started: 29 January 2024

coarse-grained igneous rocks used as building stones. Journal of Archaeological Science, **129**, doi: 10.1016/j.jas.2021.105376.

Uchida, E., Ogawa, Y., Maeda, N. & Nakagawa, T. 2000. Deterioration of stone materials in the Angkor monuments, Cambodia. Engineering Geology, **55**, 101-112, doi: Doi 10.1016/S0013-7952(99)00110-6.

Underwood, S.J., Schultz, M.D., Berti, M., Gregoretti, C., Simoni, A., Mote, T.L. & Saylor, A.M. 2016. Atmospheric circulation patterns, cloud-to-ground lightning, and locally intense convective rainfall associated with debris flow initiation in the Dolomite Alps of northeastern Italy. Natural Hazards and Earth System Sciences, **16**, 509-528, doi: 10.5194/nhess-16-509-2016.

Wang, D., Li, X.-b., Peng, K., Ma, C., Zhang, Z. & Liu, X. 2018. Geotechnical characterization of red shale and its indication for ground control in deep underground mining. Journal of Central South University, **25**, 2979-2991, doi: 10.1007/s11771-018-3968-4.

Wang, F.W., Chen, Y., Peng, X.L., Zhu, G.L., Yan, K.M. & Ye, Z.H. 2022. The fault-controlled Chengtian landslide triggered by rainfall on 20 May 2021 in Songyang County, Zhejiang Province, China. Landslides, **19**, 1751-1765, doi: 10.1007/s10346-022-01891-x.

Wang, M., Qi, Y.A., Li, D., Dai, M.Y. & Chang, Y.G. 2014. Ichnofabrics and Their Environmental Interpretation from the Fluvial Deposits of the Middle Triassic Youfangzhuang Formation in Western Henan, Central China. Journal of Earth Science, **25**, 648-661, doi: 10.1007/s12583-014-0454-2.

Wang, Y., Liu, J., Yan, S., Yu, L. & Yin, K. 2017. Estimation of probability distribution of shear strength of slip zone soils in Middle Jurassic red beds in Wanzhou of China. Landslides, **14**, 2165-2174, doi: 10.1007/s10346-017-0890-z.

Wankmuller, C., Kunovjanek, M. & Mayrgundter, S. 2021. Drones in emergency response-evidence from cross-border, multi-disciplinary usability tests. International Journal of Disaster Risk Reduction, **65**, doi: 10.1016/j.ijdrr.2021.102567.

Wild, K.M., Walter, P. & Amann, F. 2017. The response of Opalinus Clay when exposed to cyclic relative humidity variations. Solid Earth, **8**, 351-360, doi: 10.5194/se-8-351-2017.

Wu, L.Z., Zhang, L.M., Zhou, Y., Xu, Q., Yu, B., Liu, G.G. & Bai, L.Y. 2018. Theoretical analysis and model test for rainfall-induced shallow landslides in the red-bed area of Sichuan. Bulletin of Engineering Geology and the Environment, **77**, 1343-1353, doi: 10.1007/s10064-017-1126-0.

https://doi.org/10.5194/egusphere-2023-2590
Preprint. Discussion started: 29 January 2024

Xia, K.Z., Chen, C.X., Zheng, Y., Zhang, H.N., Liu, X.M., Deng, Y.Y. & Yang, K.Y. 2019. Engineering geology and ground collapse mechanism in the Chengchao Iron-ore Mine in China. Engineering Geology, **249**, 129-147, doi: 10.1016/j.enggeo.2018.12.028.

Xue, Y., Wang, Q., Ma, L., Yu, Y. & Zhang, R. 2023. Mechanisms and controlling factors of heave in summer for high-speed railway cutting: A case study of Northwest China. Construction and Building Materials, **365**, doi: 10.1016/j.conbuildmat.2022.130061.

Yan, L.B., Peng, H., Zhang, S.Y., Zhang, R.X., Kasanin-Grubin, M., Lin, K.R. & Tu, X.J. 2019. The Spatial Patterns of Red Beds and Danxia Landforms: Implication for the formation factors-China. Scientific Reports, **9**, doi: 10.1038/s41598-018-37238-7.

Yang, Y., Zhou, J., Xu, F. & Xing, H. 2016. An Experimental Study on the Water-Induced Strength Reduction in Zigong Argillaceous Siltstone with Different Degree of Weathering. Advances in Materials Science and Engineering, doi: 10.1155/2016/4956986.

Yao, H., Jia, S., Gan, W., Zhang, Z. & Lu, K. 2016. Properties of Crushed Red-Bed Soft Rock Mixtures Used in Subgrade. Advances in Materials Science and Engineering, **2016**, doi: 10.1155/2016/9624974.

Zha, F., Huang, K., Kang, B., Sun, X., Su, J., Li, Y. & Lu, Z. 2022. Deterioration Characteristic and Constitutive Model of Red-Bed Argillaceous Siltstone Subjected to Drying-Wetting Cycles. Lithosphere, **2022**, doi: 10.2113/2022/8786210.

Zhang, M., Yin, Y. & Huang, B. 2015. Mechanisms of rainfall-induced landslides in gently inclined red beds in the eastern Sichuan Basin, SW China. Landslides, **12**, 973-983, doi: 10.1007/s10346-015-0611-4.

Zhang, S., Xu, Q. & Hu, Z.M. 2016. Effects of rainwater softening on red mudstone of deep-seated landslide, Southwest China. Engineering Geology, **204**, 1-13, doi: 10.1016/j.enggeo.2016.01.013.

Zhang, Y., Li, F. & Chen, J. 2008. Analysis of the interaction between mudstone and water. Journal of Engineering Geology, **16**, 22-26.

Zhang, Z., Gao, W., Zeng, C., Tang, X. & Wu, J. 2020. Evolution of the disintegration breakage of red-bed soft rock using a logistic regression model. Transportation Geotechnics, **24**, doi: 10.1016/j.trgeo.2020.100382.

Zhang, Z.H., Chen, X.C., Yao, H.Y., Huang, X. & Chen, L.W. 2021. Experimental Investigation on Tensile Strength of Jurassic Red-Bed Sandstone under the Conditions of Water Pressures and Wet-Dry Cycles. Ksce Journal of Civil Engineering, **25**, 2713-2724, doi: 10.1007/s12205-021-1404-z.

https://doi.org/10.5194/egusphere-2023-2590
Preprint. Discussion started: 29 January 2024

Zhang, Z.L., Wang, T., Wu, S.R., Tang, H.M. & Liang, C.Y. 2017. The role of seismic triggering in a deep-seated mudstone landslide, China: Historical reconstruction and mechanism analysis. Engineering Geology, **226**, 122-135, doi: 10.1016/j.enggeo.2017.06.001.

Zhao, M., Liu, X. & Su, Y. 2005. Experimental studies on engineering properties of red bed material containing slaking rock. Chinese Journal of Geotechnical Engineering, **27**, 667-671.

Zhou, C., Liu, Z., Xue, Y., Li, Y., Fan, X., Chen, W. & Sun, P. 2023. Some thoughts on basic research of red beds disaste. Journal of Engineering Geology, **31**, 689-705, doi: 10.13544/j.cnki.jeg.2022-0842.

Zhou, C., Yu, L., Huang, Z., Liu, Z. & Zhang, L. 2021. Analysis of microstructure and spatially dependent permeability of soft soil during consolidation deformation. Soils and Foundations, **61**, 708-733, doi: https://doi.org/10.1016/j.sandf.2021.02.004.

Zhu, B., Hu, H. & Chen, Q. 2003. Preliminary study on the characteristics and hazards of M - shaped roadcut slope in red beds. Journal of Engineering Geology, **11**, 411-415.